JOURNAL OF PROPULSION AND POWER
Vol. 12, No. 3, May–June 1996

Advanced Propeller Performance Calculation by a Lifting Surface Method

Johan B. H. M. Schulten*
National Aerospace Laboratory, 8300 AD Emmeloord, The Netherlands

The application of a lifting surface theory to compute the aerodynamics of advanced propellers is studied. Starting from the inviscid, compressible flow equations for a perturbed, axially subsonic flow, expressions are derived for the velocity field of a propeller. By using a representation of Green's function in separated, cylindrical coordinates, the radial boundary condition at the hub is naturally incorporated in the velocity field. Application of the boundary condition at the blade surfaces yields an integral equation for the unknown pressure jump distribution over the blades. A Galerkin projection transforms this integral equation into a set of linear equations, which is solved numerically. Comparison with experimental data shows that the gradients of thrust and power coefficients vs the advance ratio at the windmilling point are accurately predicted. By taking into account some higher-order effects in the geometry description of the blades, and by application of the so-called leading-edge suction analogy, a good agreement between theory and experiment is maintained up to high aerodynamic loading.

Nomenclature

B = number of blades
C_P = shaft power coefficient
C_T = thrust coefficient
$c(\rho)$ = blade chord
$\bar{c}(\rho)$ = axial extent of blade chord
c_∞ = ambient speed of sound
$D(r)$ = angular position of zeroth blade at $t = 0$, $x = 0$, Eq. (4)
$g_0(r)$ = vector normal to blade helical surface, Eq. (9)
$H_m^{(2)}$ = second kind Hankel function of order m
h = hub/tip ratio
i_x, i_r, i_θ = unit vectors in x, r, θ directions, Fig. 2
J = advance ratio, $\pi M/|\Omega|$
J_m = Bessel function of the first kind of order m
k = circumferential periodicity of incident velocity
M = axial flow Mach number, Fig. 2
$M_n(r)$ = helical Mach number component normal to leading edge, Eq. (20)
$n_0(r)$ = unit normal on blade helical surface, Eq. (15)
P_{vA} = blade loading coefficient, Eq. (16)
p = pressure induced by blade row
Q = displacement source strength
R_m = reduced Green's function, Eq. (5)
r = radial coordinate, Fig. 2
$S_h(x)$ = hub contour function, Eq. (10)
t = time coordinate
v = velocity induced by blade row
x = axial coordinate
α = axial wave number, Eq. (3)
$\beta(r)$ = blade angle distribution, Fig. 3
γ = radial wave number, Eq. (5)
Δp = blade pressure jump distribution, Eq. (8)
$\Delta\phi(x, r)$ = angular blade thickness, Fig. 3
ε = small perturbation parameter
η = propulsion efficiency, JC_T/C_P
θ = circumferential coordinate, Fig. 2, projection variable, Eq. (26)
ξ = axial source coordinate, Fig. 2
ρ = radial source coordinate, density
τ = source time
ϕ = circumferential source coordinate, Fig. 2, normalized chordwise coordinate, Eq. (18)
Ω = tangential tip Mach number, Fig. 2

Subscripts
F = force
h = hub
L = leading edge
Q = displacement
T = trailing edge
∞ = ambient, at infinity

Superscripts
(a) = anechoic
$+$ = blade lower side
$-$ = blade upper side
$\sim$ = in physical domain

Symbol
$\langle\cdot\rangle$ = inner product of two three-dimensional vectors

Received May 22, 1995; presented as Paper 95-3035 at the AIAA/ASME/SAE/ASEE 31st Joint Propulsion Conference and Exhibit, San Diego, CA, July 10–12, 1995; revision received Dec. 22, 1995; accepted for publication Jan. 4, 1996.

*Senior Research Engineer, Aeroacoustics Department, P.O. Box 153. Senior Member AIAA.

Introduction

TRIGGERED by the sharp rise of the fuel cost in the mid-1970s the interest in the classical way of aircraft propulsion revived. Since then, it has been well established[1] that propellers of modern design can operate with a substantially higher fuel efficiency than turbofan engines, even at high subsonic flight speed. Potential cabin noise problems and the return to relatively modest fuel prices have hampered a breakthrough of these advanced high-speed propellers. However, in the long run, more efficient propulsion systems will inevitably become of crucial importance. Meanwhile, commuter and general aviation aircraft, traditionally equipped with propellers, have already benefited from the research on high-speed propellers and are more and more showing blade shape refinements clearly influenced by the research on advanced propellers.

The high subsonic cruise speed regime in which advanced propellers are designed to operate necessarily involves super-

sonic helical tip speeds. Therefore, a high efficiency can only be achieved by the application of very thin, highly swept blades. A maximum thickness of only 2% of the chord in the outer part of the blade span, say beyond 70%, is standard. Further, a radially varying leading-edge sweep angle up to 45 deg helps to minimize the unfavorable effects of wave drag (Fig. 1). In general, the blade geometry of an advanced high-speed propeller is designed such that the entire leading edge from hub to tip remains effectively subsonic, i.e., the relative Mach number component normal to the leading edge is less than unity. In addition, a rather high number of wide-chord blades, typically eight, is chosen to obtain a fairly smooth distribution of air loading over the propeller volume swept by the blades. As a result, the distortions of the oncoming flow by the blades remain relatively small, at least under cruise conditions. According to classical actuator disc theory, a low distortion level is directly related to a high propulsion efficiency.

These conditions also have relevance to the potential success of methods to compute the flow about advanced propellers. In the past 20 years, lifting line, lifting surface, Euler, and Navier–Stokes methods have been applied to advanced propellers with varying degrees of success. In the mentioned order these methods model the flow more and more realistically and should, strictly speaking, yield progressively more accurate results. However, this is not always the case since discretization errors in the numerical schemes of the Euler and Navier–Stokes methods, such as numerical dissipation and dispersion, adversely affect the accuracy of the solution. As shown by Nallasamy et al.,[2] two Euler methods can yield significantly different solutions for the same case and, moreover, both also different from experimental values.

The lifting line method implies the most drastic approximation. Although shown to be a very useful model for conventional propellers by Brouwer,[3] it is of limited use for advanced propellers, mainly because it requires a high aspect ratio of the blades, a feature not particularly characteristic for advanced propellers. Furthermore, most lifting line methods do not allow supersonic helical tip speed and blade sweep.

Lifting surface methods are based on the assumption of small, inviscid perturbations of a uniform main flow. Under this assumption the compressible flow equations become linear in the perturbed variables. Since there are, in principle, no restrictions to the blade planform, the lifting surface approximation seems to be suitable for low aspect ratio, highly swept advanced propellers.

Euler methods remove the limitation to small perturbations at the price of a considerable increase in computing cost compared to the aforementioned methods. They are able to compute nonlinear phenomena like transonic shocks in the blade passages that may occur at high subsonic speeds.

Finally, the Navier–Stokes methods include also the effects of viscosity, which are essential to describe phenomena like flow separation.

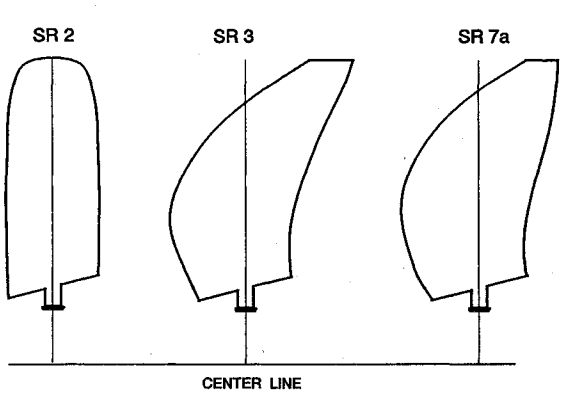

Fig. 1 NASA research advanced propeller blade planforms. The SR2 was made for comparison purposes only.

This article presents the application of a lifting surface method[4] to the computation of the aerodynamics of advanced propellers. Although several lifting surface methods[5–8] have been presented over the years, the appropriateness to compute performance data has remained somewhat unclear, and relatively large discrepancies were reported by Hwang[6] and Hanson.[9] The present method is the first lifting surface method to include the presence of the hub in the analysis, i.e., the boundary condition at the hub, here approximated by an infinite cylinder. At the same time the displacement velocity of the actual, variable diameter spinner–hub assembly is included as an external, incident field. The method also includes the effect of velocity induced by the blade thickness distribution, a mechanism first noted for propellers by Van de Vooren and Zandbergen[10] and ignored in most lifting surface methods.

The primary unknown quantity in the lifting surface problem is the pressure jump distribution over the blades. Once this has been found, it seems straightforward to compute the thrust C_T and power C_P coefficients. However, these coefficients, in terms of which most of the experimental results are presented, are in a linearized theory not uniquely determined with respect to higher-order terms. At higher loading these terms do affect the aerodynamic coefficients. The modeling of higher-order terms refers to questions as 1) should the camber of the blades be included, or 2) may the blades be approximated by uncambered sheets aligned with the undisturbed flow, and 3) should a leading-edge suction force be restored from the computed pressure jump distribution that acts only normal to the blade camber surface. Strictly speaking, one should be satisfied when the lifting surface theory predicts the gradients of C_T and C_P vs J at the unloaded condition, i.e., the windmilling point, correctly. It is, however, of practical interest to explore how far the applicability of the lifting surface method can be extended.

The fact that only a few percent of the computing costs of an Euler method are needed for the present lifting surface method, makes it an affordable tool for parametric studies.

Analysis

Governing Equations

The lifting surface modeling of the present problem is based on two assumptions. First, the viscosity of the flow is considered to be small, i.e., the Reynolds number is assumed to be sufficiently high. Secondly, the perturbations of the main flow caused by the presence of the blades are supposed to be relatively small.

The problem is formulated in a nonrotating, stationary frame of reference in which the position of the blades is time dependent. We consider a single propeller placed in a uniform, compressible subsonic main flow of Mach number M ($0 < M < 1$). There is, however, no such limitation to the angular speed of the propeller, and tip speeds may be well in the supersonic regime. To obtain a nondimensional formulation, the mass density ρ_∞ and speed of sound c_∞ of the main flow and the blade tip radius are taken as scaling parameters. With this scaling the pressure and density perturbation become leading-order identical. If the x axis is chosen with the positive direction downstream along the propeller axis (Fig. 2), the governing, i.e., the leading-order, flow equations are the linearized Euler equations for the (dimensionless) perturbation pressure $\tilde{p}$ and velocity $\tilde{\mathbf{v}}$

$$\frac{D\tilde{p}}{Dt} + \langle \nabla \cdot \tilde{\mathbf{v}} \rangle = 0 \tag{1}$$

$$\frac{D\tilde{\mathbf{v}}}{Dt} + \nabla \tilde{p} = \mathbf{0} \tag{2}$$

where the linearized material derivative $D/Dt = \partial/\partial t + M\partial/\partial x$.

As shown previously,[4,11] the application of generalized functions and elimination of the velocity from Eqs. (1) and (2) yields a nonhomogeneous convected-wave equation in the

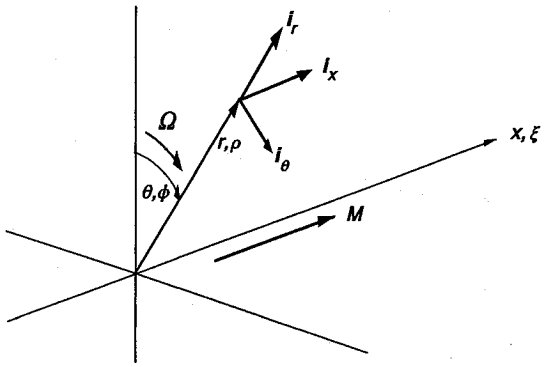

Fig. 2 Coordinate system.

pressure. The right-hand side (RHS) of this equation consists of two source terms, one of which contains the blade loading distribution and the other the blade thickness distribution. After the construction of a Green's function for this equation in terms of a multiple Fourier transform, the pressure field of the complete propeller can be expressed as an integral over the volume swept by the propeller. This pressure field contains a steady and unsteady, i.e., acoustic, components at multiples of the blade passing frequency. Upon substitution of the pressure field, the momentum equation yields expressions for the velocity induced by blade displacement and the blade loading velocity.

Blade Geometry

The angular coordinate of the leading edge of the zeroth blade at $t = 0$ is given by $\phi_L(r)$, while $x_L(r)$ denotes its axial inate (Fig. 3). The mean camber line of the blade section at radius r relative to the undisturbed helical line is denoted by ϕ_c, whereas $\Delta\phi$ describes the blade thickness in the angular coordinate. Note that ϕ_c also includes the angle of attack of the blade section. Both ϕ_c and $\Delta\phi$ are of $\mathcal{O}(\varepsilon)$.

Blade Displacement Velocity Field

In Ref. 4 it is shown that the displacement velocity field of a complete propeller is given by

$$\tilde{v}_Q = \frac{-iBM}{(2\pi)^2}\sum_{n=-\infty}^{\infty}\exp[im(\theta-\Omega t)]\int_{-\infty}^{\infty}\exp(i\alpha x)\times\begin{bmatrix}\alpha\\ -\dfrac{i\partial}{\partial r}\\ \dfrac{m}{r}\end{bmatrix}\int_h^1 R_m(\alpha, r, -m\Omega|\rho)\exp[-imD(\rho)]\times\int_{x_L(\rho)}^{x_T(\rho)}\exp\left[i\left(\frac{m\Omega}{M}-\alpha\right)\xi\right]\rho\frac{\partial\Delta\phi}{\partial\xi}\,d\xi\,d\rho\,d\alpha \tag{3}$$

where $m = -nB$, and

$$D(r) = \phi_L(r) + (\Omega/M)x_L(r) \tag{4}$$

is the angular position of the helical surface associated with the zeroth blade at $t = 0$, $x = 0$.

The reduced Green's function[4,11] R_m in Eq. (3) reads

$$R_m = R_m^{(a)} + i\frac{\pi}{2}\frac{J_m'(\gamma h)}{H_m^{(2)'}(\gamma h)}H_m^{(2)}(\gamma\rho)H_m^{(2)}(\gamma r) \tag{5}$$

where the second term in the RHS represents the hub influence, and where the anechoic part $R_m^{(a)}$ is given by

$$R_m^{(a)} = -i(\pi/2)[J_m(\gamma r)H_m^{(2)}(\gamma\rho)H(\rho-r) + J_m(\gamma\rho)H_m^{(2)}(\gamma r)H(r-\rho)] \tag{6}$$

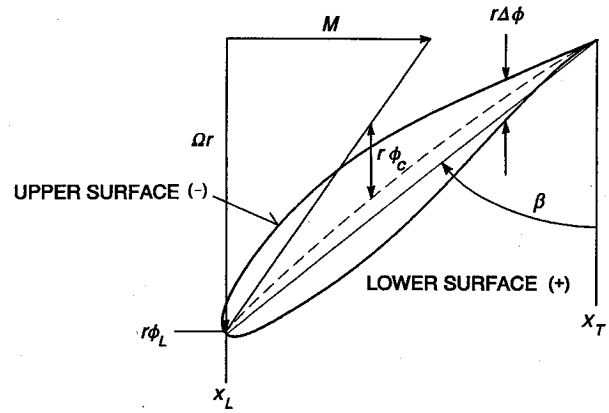

Fig. 3 Blade intersection with cylindrical surface (r = const); for clarity $\Delta\phi$ and ϕ_c have been exaggerated with respect to realistic situations.

In Eqs. (5) and (6) γ is a complex function defined in Refs. 4 and 11.

Blade Loading Velocity Field

The blade loading velocity field is given by[4]

$$\tilde{v}_F = \frac{B}{(2\pi)^2 M}\sum_{n=-\infty}^{\infty}\exp[im(\theta-\Omega t)]\int_{-\infty}^{\infty}\frac{\exp(i\alpha x)}{i[\alpha-(m\Omega/M)]}\times\int_h^1\exp[-imD(\rho)]\rho\left\{g_0(\rho)\frac{\delta(r-\rho)}{r}-\begin{bmatrix}\alpha\\ -\dfrac{i\partial}{\partial r}\\ \dfrac{m}{r}\end{bmatrix}\times\left\langle g_0(\rho)\cdot\begin{bmatrix}\alpha\\ \dfrac{i\partial}{\partial\rho}\\ \dfrac{m}{\rho}\end{bmatrix}\right\rangle R_m(\alpha, r, -m\Omega|\rho)\right\}\times\int_{x_L(\rho)}^{x_T(\rho)}\exp\left[i\left(\frac{m\Omega}{M}-\alpha\right)\xi\right]\Delta p(\xi,\rho)\,d\xi\,d\rho\,d\alpha \tag{7}$$

where the pressure jump distribution

$$\Delta p(\xi,\rho) = p^+(\xi,\rho) - p^-(\xi,\rho) \tag{8}$$

and the vector normal to the undisturbed helical surfaces

$$\boldsymbol{g}_0(r) = (\Omega/M)\boldsymbol{i}_x - D'(r)\boldsymbol{i}_r + (1/r)\boldsymbol{i}_\theta \tag{9}$$

from which it is obvious that for blades without lean, i.e., $D(r)$ constant, the radial component of $\boldsymbol{g}_0$ vanishes. To avoid bending stresses by centrifugal loads, propeller blades have zero or negligible lean.

In general, $m = k - nB$. In the present case of propeller performance computation, only $k = 0$ fields are relevant.

Hub Displacement Velocity Field

The effect of the presence of the hub is twofold. First, the induced velocity field of the propeller satisfies the radial boundary condition $v_r = 0$ at an idealized, infinite hub cylinder of radius h. Secondly, the actual hub is, in general, a slender body of revolution of variable cross section that displaces the oncoming flow radially. For propeller blades without lean this radial velocity has no effect on the loading. However, the displacement is accompanied by a perturbation of the axial velocity and this component alters the local angle of attack along

the blade. As a result, the blade loading changes correspondingly.

To model this effect, the hub is, temporarily, replaced by a source strength distribution. If the hub radius contour is denoted by $h(x)$, it is, using the technique described in Refs. 4 and 11, not difficult to show that the leading-order displacement source strength is given by

$$Q\delta(S_h) = M\frac{dh}{d\xi}\,\delta[\rho - h(\xi)] \tag{10}$$

Substitution of this source strength in the general expression for the displacement velocity[4,11] yields, after transformation to the physical domain and integration over the source region,

$$\tilde{v}_{Q,h} = -i\frac{M}{2\pi}\int_{-\infty}^{\infty}\int_{-\infty}^{\infty} h\frac{dh}{d\xi}\left\{\alpha R_0^{(a)}[\alpha, r, 0|h(\xi)]i_x - i\frac{\partial R_0^{(a)}[\alpha, r, 0|h(\xi)]}{\partial r}i_r\right\}\exp[i\alpha(x-\xi)]\,d\xi\,d\alpha \tag{11}$$

which may be further simplified by concentrating all source strength on the hub axis, i.e., replacing $R_0^{(a)}[\alpha, r, 0|h(\xi)]$ by $R_0^{(a)}[\alpha, r, 0|0]$. Then, the expression of the hub displacement velocity reduces to

$$\tilde{v}_{Q,h} = -\frac{M}{4}\int_{-\infty}^{\infty}\int_{-\infty}^{\infty} h\frac{dh}{d\xi}\,[\alpha H_0^{(2)}(\gamma r)i_x - i\gamma H_0^{(2)'}(\gamma r)i_r] \times \exp[i\alpha(x-\xi)]\,d\xi\,d\alpha \tag{12}$$

Integral Equation

In the previous sections expressions for the velocity induced by a propeller have been derived. The only unknown quantity in these expressions is Δp in the blade loading velocity [Eq. (7)]. To solve Δp we have to apply the boundary condition at the blade surfaces. The time-dependent position of the helical surface of the zeroth blade is given by

$$\phi_0(x, r, t) = D(r) + \Omega t - (\Omega/M)x \tag{13}$$

The boundary condition at the blade surfaces is written in such a way that the RHS depends solely on known quantities. Combining the boundary conditions at upper and lower blade surfaces as in Ref. 4, we obtain the following integral equation for Δp:

$$[\langle \boldsymbol{n}_0\cdot\tilde{\boldsymbol{v}}_F\rangle]_{\theta=\phi_0} = \left(\frac{M}{\|\boldsymbol{g}_0\|}\frac{\partial\phi_c}{\partial x} - \langle \boldsymbol{n}_0\cdot\tilde{\boldsymbol{v}}_Q\rangle - \langle \boldsymbol{n}_0\cdot\tilde{\boldsymbol{v}}_{Q,h}\rangle\right)_{\theta=\phi_0} \tag{14}$$

where the unit vector normal to the blades $\boldsymbol{n}_0$ is given by

$$\boldsymbol{n}_0 = \boldsymbol{g}_0(r)/\|\boldsymbol{g}_0(r)\| \tag{15}$$

Note that by the substitution of Eq. (13) for θ, which comes down to rotating with the blade, Eq. (14) becomes time independent.

The integral equation [Eq. (14)] shows that the velocity $\tilde{v}_F$ induced by the pressure jump depends on the following three quantities: 1) the blade camber and angle of attack via $\phi_c(x, r)$; 2) the blade thickness induced velocity $\tilde{v}_Q(x, r)$; and 3) the incident hub displacement velocity $\tilde{v}_{Q,h}(x, r)$.

Numerical Solution Procedure

Representation of the Pressure Jump Distribution

The first step towards the numerical solution of the integral equation derived in the previous section is the choice of a suitable description of the unknown pressure jump distribution. Basically, there are two different ways to approximate Δp: by local or by global functions. If local functions are chosen, the complete blade surface of the blade is divided into subdomains, typically trapezoidal panels, to each of which a local function is allocated. The advantage of local functions is that the integration over the blade becomes relatively simple. However, a large number of panels is generally required for an accurate solution. If the kernel of the integral equation is easily computed, this is not necessarily a drawback.

For a kernel as complicated as in the present case it is worthwhile to seek a method that requires less kernel evaluations. In principle, this can be achieved by approximating Δp by global basis functions, also called loading or trial functions, which are valid over the complete blade surface. In a symbolic notation:

$$\Delta p(\xi, \rho) = \sum_{\nu=0}^{\infty}\sum_{\lambda=0}^{\infty} P_{\nu\lambda}R_\nu(\rho)X_\lambda(\xi) \tag{16}$$

To obtain a rapid convergence of this double series it is essential to incorporate in this description the expected behavior of the solution in the neighborhood of the edges of the domain.

If the approximation is successful, the series in Eq. (16) can be truncated after a sufficiently high number of terms, viz., ν_{max} and λ_{max}, with negligible loss of accuracy.

Chordwise Representation

It is shown in Ref. 4 that for subsonic leading and trailing edges an appropriate choice for the chordwise functions is the series,

$$\Delta p = P_0\tan\frac{\phi}{2} + \sum_{\lambda=1}^{\infty} P_\lambda \sin\lambda\phi \tag{17}$$

where ϕ is related to ξ by

$$\xi = [x_T(\rho) + x_L(\rho)]/2 + [\bar{c}(\rho)/2]\cos\phi \tag{18}$$

This representation incorporates the usual subsonic square root leading-edge singularity as well as a Kutta condition behavior at the trailing edge.

However, for propfans under cruise conditions the normal situation is mixed; a subsonic leading edge throughout the blade span and a supersonic trailing edge along the outer part of the span. Then, in the outer part the following description is appropriate:

$$\Delta p = \frac{P_0}{\cos(\phi/2)} + \cos\left(\frac{\phi}{2}\right)\sum_{\lambda=1}^{\infty} P_\lambda\frac{\sin\lambda\phi}{\sin\phi} \tag{19}$$

Leading-Edge Suction Force

Within the lifting surface approximation the forces acting on the flow correspond to the pressure jump over the blades. As a result, these forces point in the direction normal to the lifting surface. However, for airfoils at an angle of attack in a subsonic, inviscid flow, a leading-edge suction force arises to achieve zero drag. This leading-edge suction force is not captured if the thrust and shaft power are computed by integrating the pressure jump over the blades. The suction force can, however, be recovered by applying locally the two-dimensional potential theory of a semi-infinite plate. From the Blasius theorem[12] and a Prandtl–Glauert transformation to include linear compressibility, it follows that the suction force X is given by

$$X = \frac{\pi}{4}\frac{1-M_n^2}{M_n^2}\lim_{x\downarrow 0}[\sqrt{x}\Delta p(x)]^2\frac{c}{2} \tag{20}$$

where M_n is the local helical velocity component normal to the leading edge (Fig. 4), and x denotes the local coordinate normal to the leading edge and tangent to the helical surface.

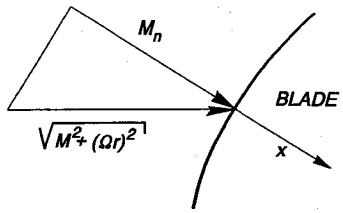

Fig. 4 Effective local Mach number in the vicinity of an edge.

Substitution of the Δp representation of Eq. (17), or alternatively Eq. (19), yields

$$X(\rho) = (\pi/4)[1/M_n^2(\rho) - 1]P_0^2(\rho)c(\rho) \tag{21}$$

where $c(\rho)$ is the local blade chord. Note that the suction force indeed is a higher-order effect since it scales on the square of the P_0 coefficient.

Spanwise Representation

Since we consider propellers at subsonic forward speed, the trailing vortices of the blade system induce velocities upstream as well as downstream. Even at supersonic helical tip speed this induction is present. Therefore, analogously to a subsonic wingtip,[13] the spanwise loading behaves as

$$P_\lambda(\rho)c(\rho) \propto \sqrt{1-\rho}, \qquad \rho \uparrow 1 \tag{22}$$

Let us first consider a rounded blade tip. Then the behavior in Eq. (22) is achieved by the chord distribution $c(\rho)$, and we write $P_\lambda(\rho)$ as

$$P_\lambda(\rho) = \sum_{\nu=0}^{\infty} P_{\nu\lambda} \cos \nu\psi \tag{23}$$

where

$$\cos \psi = 2(\rho - h)/(1 - h) - 1 \tag{24}$$

For a propeller blade with a finite tip chord, the shape function should include the square root behavior at the tip. Hence, we then take

$$P_\lambda(\rho) = \sin\left(\frac{\psi}{2}\right) \sum_{\nu=0}^{\infty} P_{\nu\lambda} \cos \nu\psi \tag{25}$$

Galerkin Projection

To transform the integral equation into a finite set of $(j_{\max} + 1)(l_{\max} + 1)$ linear equations, we adopt chordwise and spanwise Galerkin projections as follows:

$$\int_0^\pi \sin(j+1)\zeta \sin\zeta \int_0^\pi \sin(l+1)\theta \sin\theta \quad \text{Eq. (14)} \quad d\theta\, d\zeta$$

$$l = 0, l_{\max}, \qquad j = 0, j_{\max} \tag{26}$$

where

$$r = (1 + h)/2 + [(1 - h)/2]\cos\zeta \tag{27}$$

$$x = [x_L(r) + x_T(r)]/2 + [\bar{c}(r)/2]\cos\theta \tag{28}$$

This projection has been chosen since its weight function $(\sin\zeta \sin\theta)$ vanishes at the blade edges.

For steady loading it has been found that only two chordwise and three spanwise projections are usually sufficient for converged C_T and C_P results.

Computation of the matrix elements by means of a Fortran program typically takes an hour on a 486/50 personal computer for a subsonic condition. Supersonic cases and extension to seven spanwise basis functions may require up to 24 h.

Comparison with Experiments

Low Speed Results

SR2 Propeller at Mach = 0.34 Forward Speed

As a first test case, the SR2 propeller (Fig. 1) is taken. Although this propeller has the same thin blade sections as the SR3 and SR7a propellers, it lacks the characteristic blade sweep. This not only provides a reference to assess the effect of blade sweep, but also allows a calculation with the lifting line approximation. In Figs. 5 and 6 a comparison is made between the present theory, a lifting line method,[3] and measurements by Stefko and Jeracki.[14]

To make a fair comparison with the lifting line method, the hub displacement and blade thickness effects, normally included in the present lifting surface results, have been suppressed in these figures. With the Δp of the lifting surface theory as a starting point, three variants to compute thrust and power are shown: a cambered geometry with and without leading-edge suction, and a blade aligned with the undisturbed helical flow. It appears that up to moderate loading all theoretical results are very close to the measurements. While the three lifting surface variants are tangent to each other in the windmilling point, the lifting line results have a slightly steeper gradient. Since the lifting line method is essentially a different modeling, one can only be surprised by the rather modest deviation for this propeller with a relatively low aspect ratio.

For increasing loading the results start to diverge. The flow aligned geometry then really overpredicts thrust and underpre-

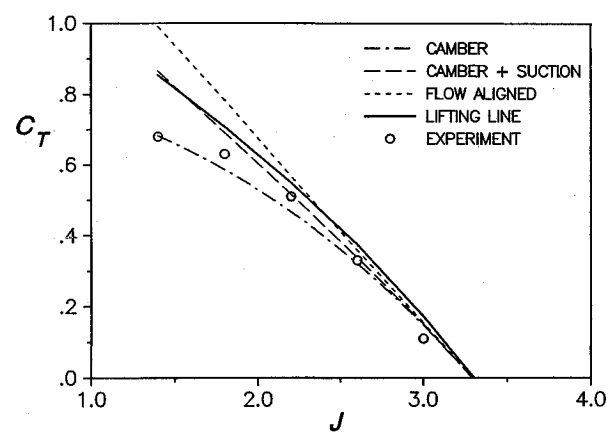

Fig. 5 Thrust without hub and blade thickness effects of SR2, $M = 0.34$, blade angle 53.8 deg ($r = 0.75$); experimental data from Ref. 14.

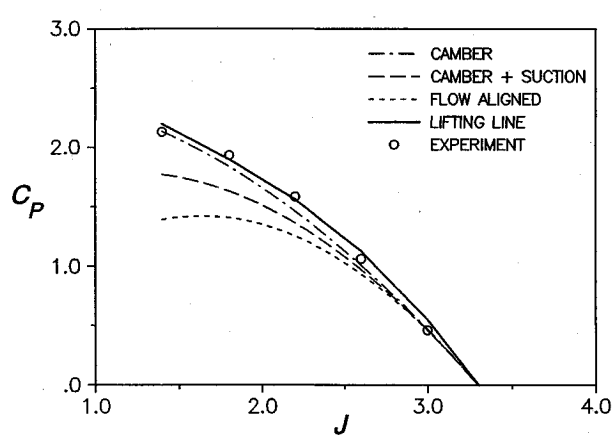

Fig. 6 Shaft power comparison of SR2, same conditions as in Fig. 5.

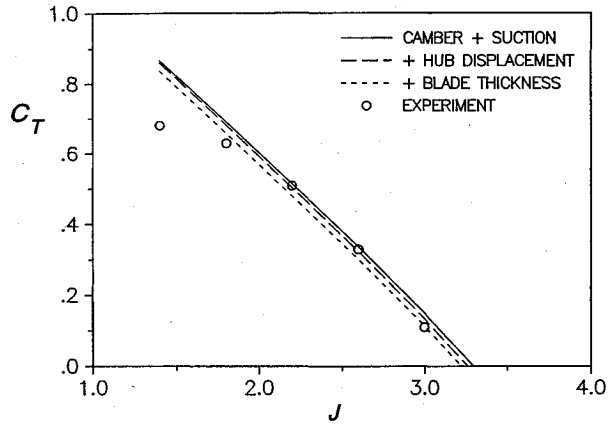

Fig. 7 Effects of hub displacement and blade thickness on thrust of SR2, same conditions as in Fig. 5.

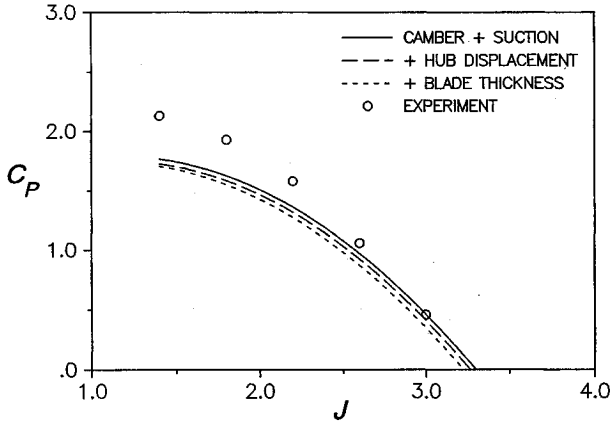

Fig. 8 Effects of hub displacement and blade thickness on shaft power of SR2, same conditions as in Fig. 5.

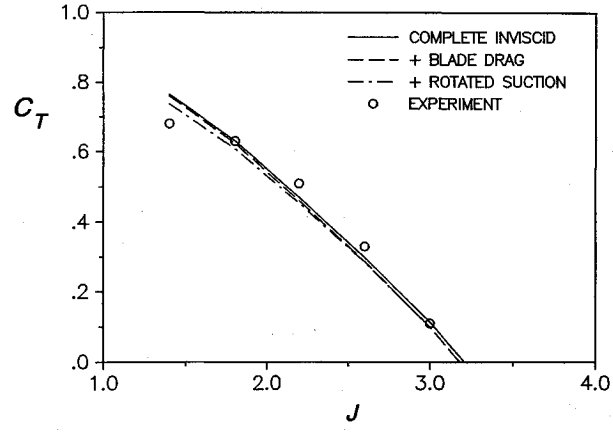

Fig. 9 Effect of idealized blade drag and suction analogy on thrust of SR2, conditions as in Fig. 5.

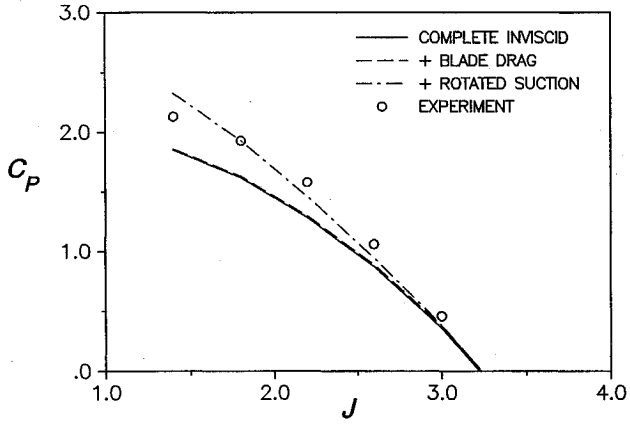

Fig. 10 Effect of idealized blade drag and suction analogy on shaft power of SR2, conditions as in Fig. 5.

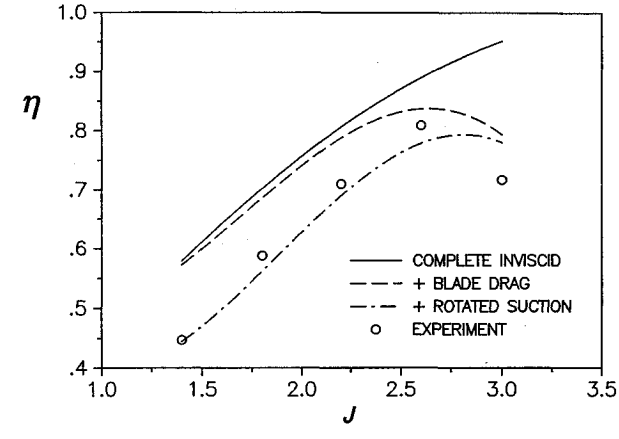

Fig. 11 Effect of idealized blade drag and suction analogy on propulsion efficiency of SR2, conditions as in Fig. 5.

dicts the shaft power, reflecting the fact that the efficiency stays invariably at unity in this modeling. The blade camber oriented modelings remain much closer to the experimental and lifting line results.

Whereas inclusion of the suction force in Figs. 5 and 6 gives a better agreement with the lifting line results for the thrust, a neglect of the suction yields a better agreement in the power.

It is interesting to see how the additional effects of hub displacement and blade thickness modify the lifting surface results. In Figs. 7 and 8 these effects have been subsequently added. The effect of hub displacement apparently is a small, but discernable reduction of the aerodynamic loading. The inclusion of blade thickness yields another reduction of the aerodynamic loading equivalent to about 0.5 deg in blade angle.

It is clear that these modifications have further improved the fit to the experimental C_T values at low loading. Still, in the high loading regime the underprediction of power remains unsatisfactory. It is well known,[15,16] however, that for the very sharp leading edge of the airfoils such as that in use for advanced propellers, a local separation occurs at the suction side that develops into a leading-edge vortex. As shown for wings by Polhamus[17] and Lamar,[18] the effect of this vortex is to swivel the leading-edge suction force over 90 deg to the suction side of the blade. This effect is the so-called leading-edge suction analogy. If this rotation of the suction force is applied in the present calculations, we observe in Figs. 9 and 10 a remarkable improvement in the power and an almost negligible change in the thrust compared to the strictly inviscid approximation.

To get an idea of the effect of blade drag, the results with an idealized drag are also shown in Figs. 9 and 10. The idealized drag is derived from the assumption of a flat plate boundary layer along the blade: turbulent on one side and laminar on the other. It is clear that the influence of blade drag is small, especially on the shaft power.

In Fig. 11 the propulsion efficiency of the SR2 is shown. Also here the suction analogy gives the best agreement with the experimental data over almost the entire loading range.

SR7a at Mach = 0.2 Forward Speed

In Fig. 12 the spanwise power distribution of the SR7a propfan is presented for typical takeoff and landing conditions. The results of the present theory are compared with Euler results of Nallasamy et al.[19] for three blade angles at a constant helical

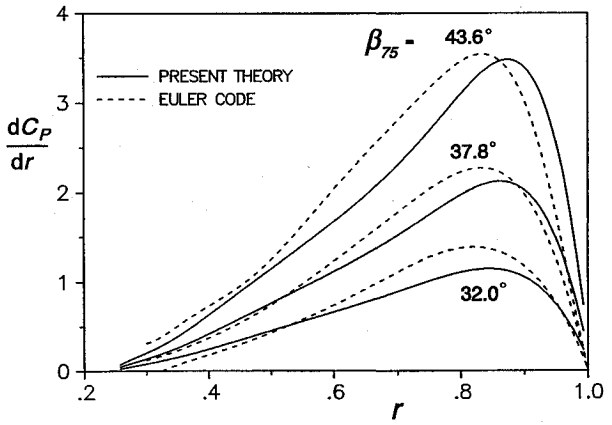

Fig. 12 Comparison of spanwise elemental power distribution of SR2 between present lifting surface method and a Euler code (Ref. 19) for three blade angles (r = 0.75), M = 0.20, and J = 0.886.

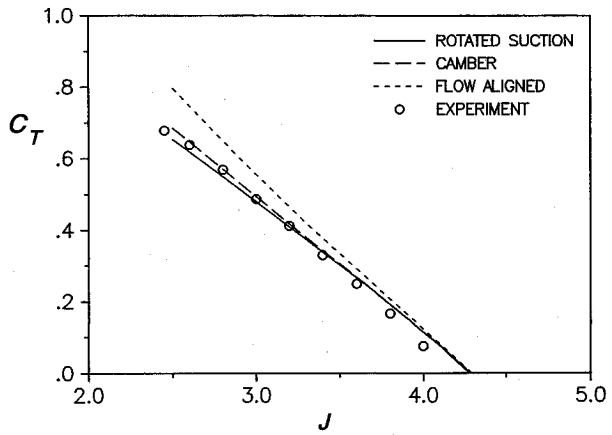

Fig. 13 Thrust of SR7a with some different modeling options, M = 0.60, blade angle 60.2 deg (r = 0.75); experimental data from Ref. 15.

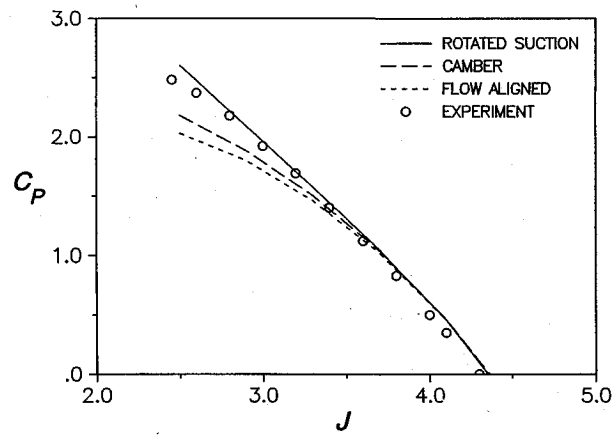

Fig. 14 Shaft power with some different modeling options, SR7a, conditions as in Fig. 13.

tip Mach number of 0.737. Although there are some discrepancies, the overall agreement is quite satisfactory, especially for the highest blade angle that is a highly loaded case.

High-Speed Results

SR7a at Mach = 0.6 Forward Speed

Whereas the previous section was concerned with propellers at low forward speed, the real interest of the method is its applicability to propellers at high forward speed.

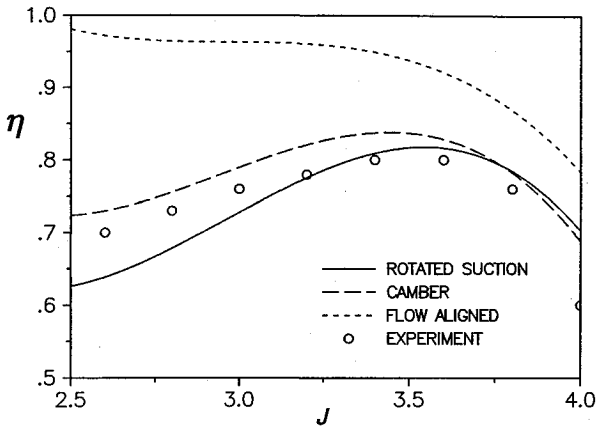

Fig. 15 Propulsion efficiency with some different modeling options, SR7a, conditions as in Fig. 13.

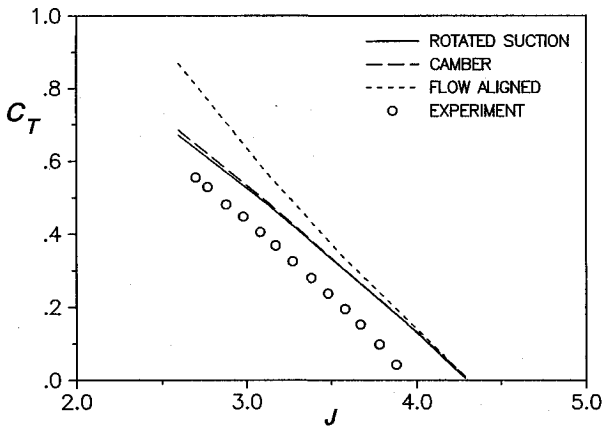

Fig. 16 Thrust with some different modeling options, SR7a, M = 0.75, blade angle = 60.2 deg (r = 0.75); experimental data from Ref. 15.

Figures 13 and 14 illustrate the application of the present method to the SR7a advanced high-speed propeller at a forward speed of M = 0.6. The very well-documented experimental results are from Stefko et al.[15] As in the previous example, a flow-aligned geometry gives the largest deviations, whereas a cambered geometry with rotated suction gives a very convincing fit to the experimental results. In this case the helical blade tip Mach number stayed just below unity at the lowest advance ratio, i.e., the highest rotational speed in this series.

The propulsion efficiency in Fig. 15 shows that the rotated suction approximation is in good agreement with the experiments in the area of maximum efficiency. For higher loading, the approximation that takes only blade camber into account is somewhat closer to the experimental data. A geometry aligned with the undisturbed flow clearly yields a far too optimistic efficiency, which only differs from unity by the presence of (idealized) blade drag.

SR7a at Mach = 0.75 Forward Speed

Although the previous example was very promising, the heaviest test of the method is for still higher Mach numbers. In Figs. 16 and 17 the results are presented for the SR7a at a forward speed of Mach number 0.75. For J below 3.5 the blade tip speed is supersonic and attains a helical Mach number of 1.18 for J = 2.60. Obviously there is a significant discrepancy with the experiments. Apparently the theory is unable to follow the shift in windmilling point from about J = 4.35 at M = 0.6 to J = 4.10 at M = 0.75 in the experiments. The downward shift beyond Mach $\approx$0.6 is believed to be a true transonic phenomenon, possibly associated with choking in the blade

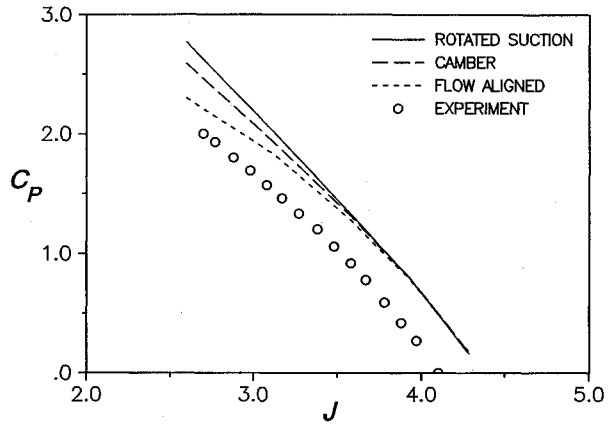

Fig. 17 Shaft power computed with some different modeling options, SR7a, conditions as in Fig. 16.

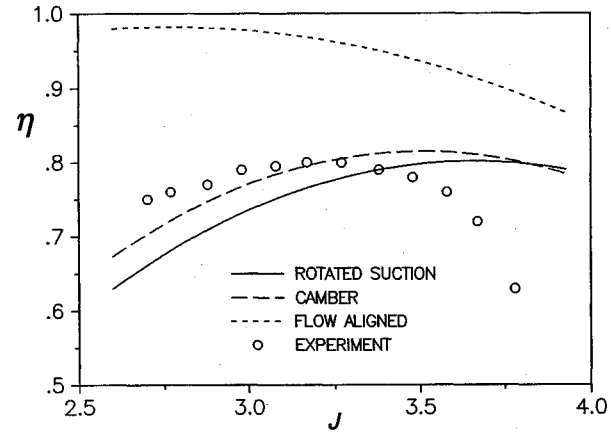

Fig. 18 Propulsion efficiency computed with some different modeling options, SR7a, conditions as in Fig. 16.

passages close to the hub. Nevertheless, the lifting surface method still predicts the thrust and power gradients quite satisfactorily for supersonic tip speeds. This indicates that the pure blade loading effect arising from an increased rotational speed is still accurately modeled by the lifting surface approximation. As shown in Fig. 18, the maximum attainable efficiency level is well predicted, albeit at a shifted advance ratio.

SR7a at Mach = 0.8 Forward Speed

To obtain more insight in the spanwise power distribution, the elemental power measured by Stefko et al.[15] in the slipstream was compared with results of the present theory in Fig. 19 for two power levels. To avoid confusion by the shift of the windmilling point discussed previously, in this figure the global power level of the theoretical results has been matched to the measured power by adjusting the blade setting angle. The agreement of the resulting spanwise power distributions with the experimental data is quite satisfactory.

SR3 at Mach = 0.8 Forward Speed

In Fig. 20 a comparison is made between experimental results for the SR3 propfan and the results of three different lifting surface methods. Obviously, the shift of the windmilling point observed for the SR7a is also found for the SR3. However, the three methods do not produce identical results. The discrepancy of Hwang's[6] results with the experimental data is the largest and corresponds to about 4 deg of blade setting angle. Although Hanson[9] accounted for blade deflection and hub blockage (using a compressible streamline curvature code), his results still show a slightly larger discrepancy with

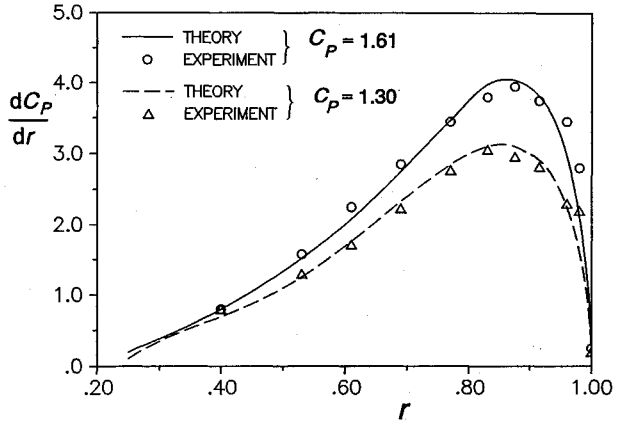

Fig. 19 Elemental spanwise power distribution SR7a, M = 0.80; experimental data from Ref. 16.

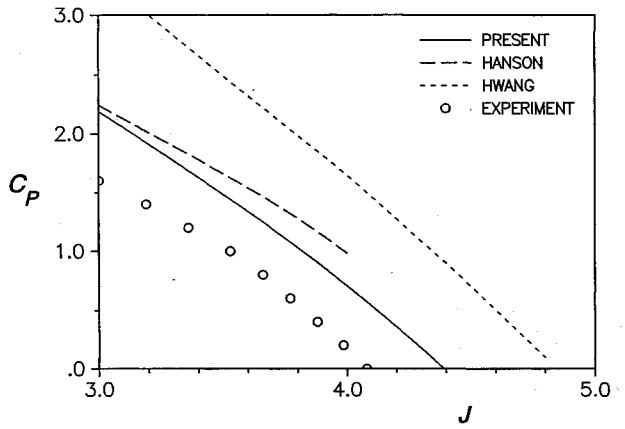

Fig. 20 Shaft power SR3, M = 0.80, blade angle 60.5 deg (r = 0.75), comparison of present theory with two other lifting surface methods (Refs. 6 and 9) and experimental data (Ref. 20).

the experiments than the present method. The discrepancy in windmilling point of the present theory and the experimental data corresponds to about 1.5 deg in blade setting angle.

Concluding Remarks

The application of a lifting surface method to the calculation of aerodynamic blade loads has been discussed. A new element in the present method is the effect of a hub. Also the effect of blade thickness that most methods ignore has been included in the analysis.

Comparison with experiments shows that the initial gradient of thrust and power coefficients is accurately predicted by the lifting surface method over a large range of forward and rotational speeds.

To extend the range of applicability of thrust and power computation a number of alternatives to include higher-order effects has been investigated. It appears that a blade camber oriented geometry and inclusion of the so-called leading-edge suction analogy to simulate the effect of a leading-edge vortex extends the range of applicability of the method to very high aerodynamic loading.

The experimentally observed shift of the windmilling point beyond $M \approx 0.6$ probably is a nonlinear, transonic phenomenon not captured by the present theory.

Acknowledgment

This work was supported under Contract 01108N by The Netherlands Agency for Aerospace Programs, NIVR.

References

[1]Hager, R. D., and Vrabel, D., "Advanced Turboprop Project," NASA SP-495, 1988.

[2]Nallasamy, N., Yamamoto, O., Warsi, S., and Bober, L. J., "Large-Scale Advanced Propeller Blade Pressure Distributions: Prediction and Data," *Journal of Propulsion and Power*, Vol. 7, No. 3, 1991, pp. 452–461.

[3]Brouwer, H. H., "On the Use of the Method of Matched Asymptotic Expansions in Propeller Aerodynamics and Acoustics," *Journal of Fluid Mechanics*, Vol. 242, Sept. 1992, pp. 117–143.

[4]Schulten, J. B. H. M., "Sound Generation by Ducted Fans and Propellers as a Lifting Surface Problem," Ph.D. Dissertation, Dept. of Applied Mathematics, Univ. of Twente, Enschede, The Netherlands, Feb. 1993.

[5]Hanson, D. B., "Unified Aeroacoustic Analysis for High Speed Turboprop Aerodynamics and Noise," *Volume I—Development of Theory for Blade Loading, Wakes, and Noise*, NASA CR 4329, March 1991.

[6]Hwang, C.-C., "Propfan Supersonic Panel Method Analysis and Flutter Predictions," Ph.D. Dissertation, Purdue Univ., West Lafayette, IN, May 1990.

[7]Chen, S. H., "Prediction of Periodic Loadings on a Single Rotation Propfan with Off-Axis Inflow," *Journal of Propulsion and Power*, Vol. 8, No. 1, 1992, pp. 144–150.

[8]Lohmann, D., "Prediction of Ducted Radiator Fan Aeroacoustics with a Lifting Surface Method," DGLR/AIAA Paper 92-02-098, May 1992.

[9]Hanson, D. B., "Compressible Lifting Surface Theory for Propeller Performance Calculation," *Journal of Aircraft*, Vol. 22, No. 1, 1985, pp. 19–27.

[10]Van de Vooren, A. I., and Zandbergen, P. J., "Noise Field of a Rotating Propeller in Forward Flight," *AIAA Journal*, Vol. 1, No. 7, 1963, pp. 1518–1526.

[11]Schulten, J. B. H. M., "Effects of Asymmetric Inflow on Near-Field Propeller Noise," *AIAA Journal*, Vol. 34, No. 2, 1996, pp. 251–258.

[12]Milne-Thomson, L. M., *Theoretical Aerodynamics*, Dover, New York, 1973.

[13]Ashley, H., and Landahl, M. T., *Aerodynamics of Wings and Bodies*, Addison–Wesley, Reading, MA, 1965.

[14]Stefko, G. L., and Jeracki, R. J., "Wind Tunnel Results of Advanced High Speed Propellers in the Takeoff, Climb, and Landing Operating Regimes," AIAA Paper 85-1259, July 1985.

[15]Stefko, G. L., Rose, G. E., and Podboy, G. G., "Wind Tunnel Performance Results of an Aeroelastically Scaled 2/9 Model of the PTA Flight Test Prop-Fan," AIAA Paper 87-1893, June 1987.

[16]Hanson, D. B., "Propeller Noise Caused by Blade Tip Radial Forces," AIAA Paper 86-1892, July 1986.

[17]Polhamus, E. C., "A Concept of the Vortex Lift of Sharp-Edge Delta Wings Based on a Leading-Edge-Suction Analogy," NASA TN D-3767, Dec. 1966.

[18]Lamar, J. E., "Prediction of Vortex Flow Characteristics of Subsonic and Supersonic Speeds," *Journal of Aircraft*, Vol. 13, No. 7, 1976, p. 490.

[19]Nallasamy, M., Woodward, R. P., and Groeneweg, J. F., "High-Speed Propeller Performance and Noise Predictions at Takeoff/Landing Conditions," *Journal of Aircraft*, Vol. 26, No. 6, 1989, pp. 563–569.

[20]Rohrbach, C., Metzger, F. B., Black, D. M., and Ladden, R. M., "Evaluation of Wind Tunnel Performance Testings of an Advanced 45° Swept Eight-Bladed Propeller at Mach Numbers from 0.45 to 0.85," NASA CR 3505, March 1982.